ChemPubSoc Europe

DOI: 10.1002/cmdc.201500575

CHEMMEDCHEM Full Papers

Fragment Screening of Soluble Epoxide Hydrolase for Lead Generation—Structure-Based Hit Evaluation and Chemistry Exploration

Yafeng Xue,*[a] Thomas Olsson,[b] Carina A Johansson,[a] Linda Öster,[a] Hans-Georg Beisel,[b] Mattias Rohman,[a] David Karis,[b] and Stefan Bäckström[a]

Soluble epoxide hydrolase (sEH) is involved in the regulation of many biological processes by metabolizing the key bioactive lipid mediator, epoxyeicosatrienoic acids. For the development of sEH inhibitors with improved physicochemical properties, we performed both a fragment screening and a high-throughput screening aiming at an integrated hit evaluation and lead generation. Followed by a joint dose–response analysis to confirm the hits, the identified actives were then effectively triaged by a structure-based hit-classification approach to three prioritized series. Two distinct scaffolds were identified as tractable starting points for potential lead chemistry work. The oxoindoline series bind at the right-hand side of the active-site pocket with hydrogen bonds to the protein. The 2-phenylbenzimidazole-4-sulfonamide series bind at the central channel with significant induced fit, which has not been previously reported. On the basis of the encouraging initial results, we envision that a new lead series with improved properties could be generated if a vector is found that could merge the cyclohexyl functionality of the oxoindoline series with the trifluoromethyl moiety of the 2-phenylbenzimidazole-4-sulfonamide series.

Introduction

The oxidation products of arachidonic acid have been established as bioactive lipid mediators and are regulators of many biological processes. These products are formed mainly by the action of three classes of enzymes: cyclooxygenases, lipoxygenases, and cytochromes. The cytochromes convert arachidonic acid into epoxyeicosatrienoic acids (EETs). EETs are considered to have several important biological functions, as they have been implicated in diverse medical conditions, including hypertension,[1] inflammation,[2] pain,[3] and the metabolic syndrome.[4] Given that EETs are mainly metabolized by the enzyme soluble epoxide hydrolase (sEH, EC 3.3.2.10), inhibition of this enzyme presents a possibility to address several pathological conditions.[5,6]

Many pharmaceutical companies have been involved in developing inhibitors of sEH, initially targeting hypertension.[7,8] The target was selected based on studies indicating that EETs were important in regulating vascular function.[9,10] Vasodilation in several organs, as a result of exposure to EETs, has been reported by a number of groups.[11–14] One of the most studied compounds for this indication is 1-(1-acetylpiperidin-4-yl)-3-adamantan-1-ylurea (AR9281, Figure 1[5,15]), which was developed by Arete Therapeutics. AR9281 was advanced into phase II clinical studies but did not progress further probably because of a lack of efficacy.[16]

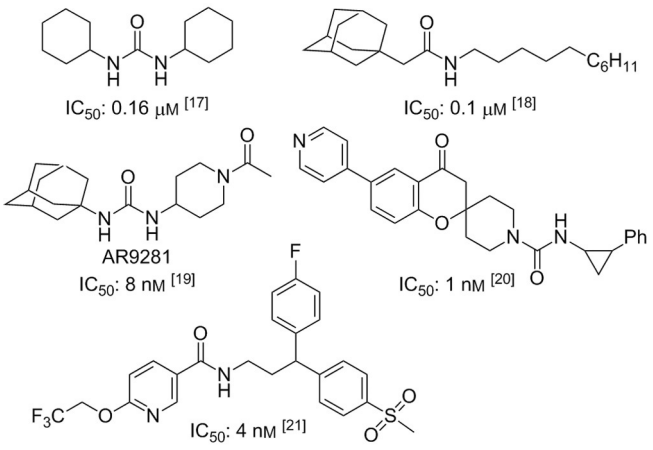

Figure 1. Representative sEH inhibitors[17–21] with their IC_{50} values for human sEH.

The structure and catalytic mechanism of sEH have been described in several reviews.[6,22] The X-ray crystal structures of sEH in complex with inhibitors show a very large binding pocket with a narrow channel in which the actual reaction occurs.[23] The catalytic site consists of two tyrosine residues

[a] Dr. Y. Xue, Dr. C. A. Johansson, Dr. L. Öster, Dr. M. Rohman, Dr. S. Bäckström
Department Discovery Sciences, AstraZeneca R&D Gothenburg
Pepparedsleden 1, 431 83 Mölndal (Sweden)
yafeng.xue@astrazeneca.com

[b] Dr. T. Olsson, Dr. H.-G. Beisel, Dr. D. Karis
Department Medicinal Chemistry, CVMD iMED
AstraZeneca R&D Gothenburg
Pepparedsleden 1, 431 83 Mölndal (Sweden)

Supporting Information for this article is available on the WWW under http://dx.doi.org/10.1002/cmdc.201500575.

(Tyr383 and Tyr466) that activate the epoxide for ring opening and an aspartate residue (Asp335) for concomitant nucleophilic attack. The ester formed is then quickly hydrolyzed to the corresponding dihydroxyeicosatrienoic acid (DHET). Essentially all published inhibitors of sEH bind to these two tyrosine residues and the aspartate residue. A key element for this binding is usually a carbonyl group of a urea or an amide, which forms hydrogen bond(s) (H-bond) to the tyrosine residue(s), and the NH group acts as a H-bond donor to the aspartate residue. Various amides and ureas have been described as sEH inhibitors (Figure 1).[17–21]

The major pharmacophores of these inhibitors are urea- and amide-based motifs (Figure 1) that bear polar interactions to the active-site residues. Other parts of the inhibitors are mostly hydrophobic and mainly have a space-filling function (i.e., van der Waals interactions), which overall renders most known sEH inhibitors as having poor physical properties. The secondary and tertiary pharmacophores include polar groups that interact with sEH outside the central channel or are in contact with the solvent.[6]

Fragment-based lead generation has been established as a mature technology for developing drug-like lead series.[24] For sEH, structure-based virtual screening (VS) was initially used for fragment work that was focused on lead generation and further medicinal chemistry expansion.[25,26] In the work of Tanaka et al.,[25] in demonstrating the great power of VS with exceptionally high hit rates, the authors noted that the hits from such work were mainly urea and amide derivatives containing diverse highly lipophilic substituents. In the case of Xing et al.,[26] the authors showed that VS could be a powerful tool in combination with combinatorial library design for efficient lead generation. Recently, various computational approaches have been employed in silico VS for fragment screening to find sEH inhibitors. In particular, a number of recent papers have illustrated how sophisticated computational regimes can be applied to sEH to enable efficient in silico fragment screening, for which a number of novel scaffolds have been identified that are distinct from the general amide and urea derivatives.[27,28] Notably, in the in silico VS performed by Moser et al.,[28] the enforced filters included one to satisfy H-bonding interactions to the active-site triad as an essential pharmacophore. Furthermore, in most of the structure-based VS procedures, the active-site pocket of sEH was treated or implied as conformationally rigid. On the other hand, experimental screening by biochemical and biophysical assays should allow sampling of a complete conformational space in addition to identifying inhibitors that bind outside the central channel. A recent example is fragment screening by X-ray crystallography with cocktail soaking, by which a secondary amine-based scaffold was found as a promising lead for further optimization.[29]

In addition to the consideration of novel intellectual property space, there is a clear need to identify distinct scaffolds with additional polar interactions (i.e., other than interactions with the active-site residues) to enable the development of sEH inhibitors with improved physicochemical properties. Therefore, we set out to find hit series with non-urea-based scaffolds for lead generation of sEH inhibitors. Herein, we present our results from a recent effort of a combined fragment screening and high-throughput screening (HTS) hit-finding approach and subsequent structure-based hit evaluation.

Results and Discussion

Early assay validation and combined fragment screening and high-throughput screening

In recent years, we have gradually adopted a holistic hit finding approach for selected feasible targets that combines fragment screening and HTS with joint chemistry efforts. The benefit of this strategy has been supported by others.[30] In the case of sEH, we had planned to run an integrated lead generation by combining fragment screening and HTS. The plan was to run a fragment screening in parallel with a HTS, which would then be followed by joint hit evaluation and chemistry expansion.

First, ligand-observed NMR spectroscopy was explored and established as the primary assay format for fragment screening (Figure 2). A total of 4056 compounds (including 2861 from a targeted selection and 1195 from a general selection) were tested in the NMR spectroscopy binding assay, which resulted

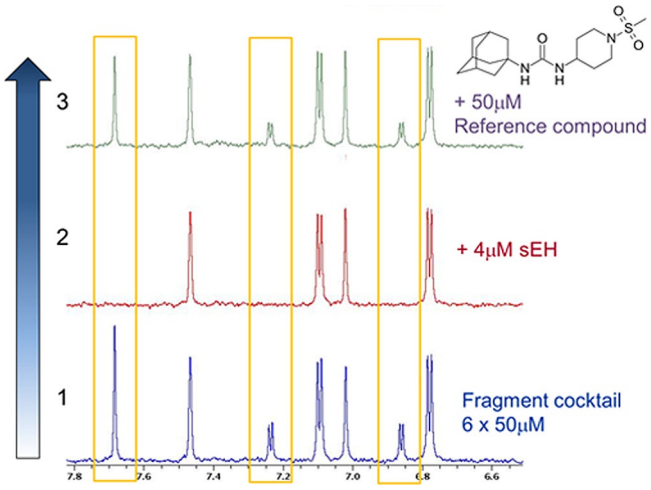

Figure 2. ^{1}H NMR signals, CPMG spectra. Signals within yellow boxes belong to fragment hit binding to sEH. 1D NMR binding assay: A competition experiment by using a known inhibitor of sEH [1-(1-adamantyl)-3-(1-methylsulfonyl-4-piperidyl)urea,[15] PDB ID: 5ALZ[32]] as the reference compound. A 1D NMR ligand-observed CPMG experiment[33] was used for detection. The assay was performed in three steps: 1) addition of a fragment mixture 2) addition of sEH protein to detect binding, and 3) addition of the reference compound to assure specific binding to the active site.

in hit rates of 17 and 27% for the targeted and general libraries, respectively. The overall hit rate was 20%. Next, we determined the initial binding affinity (K_d) by a NMR spectroscopy assay with reporter displacement[31] (Figures S2 and S3, Supporting Information). The K_d values for 300 compounds were determined to fall within the range of 0.018 to 1.5 mM (for details, see the Supporting Information). Owing to the large

volume of the active-site pocket of sEH, some of the fragment hits might not bind to the same region as the reporter molecule, which makes relevant K_d values difficult to obtain for those hits. Nonetheless, binding affinity data were obtained for the majority of the compounds tested.

In parallel, a HTS campaign was started by using a biochemical assay on an Agilent RapidFire high-throughput mass spectrometry system (RapidFire-MS, Agilent Technologies). Prior to the full execution of the HTS, we performed an extensive assay validation of the RapidFire-MS assay, including a rigorous cross validation between the fragment screening (NMR binding) and the HTS assays (Figure 3a). First, 10000 compounds were tested by using the HTS assay; this was followed by dose–response analysis of the identified actives. Interestingly, an exceptionally good recovery was obtained despite the high hit rate in the spot test. Furthermore, a subset (36 compounds) of the HTS actives was then analyzed by NMR spectroscopy, which resulted in a remarkable 92% recovery, from which 33 out of 36 compounds were confirmed as specific binders; this demonstrated the robustness of the HTS assay (Figure 3a). In a similar effort, a set of fragment hits (300 compounds) originating from the NMR spectroscopy screen were analyzed by using the HTS assay and over 66% (200 out of 300 compounds) showed inhibition within the concentration range used (up to 250 μM) (Figure 3a). Finally, IC_{50} values from the HTS assay and K_d values determined by NMR spectroscopy were compared and they displayed excellent correlation (Figure S4). Relative to RapidFire-MS, the NMR spectroscopy (reporter displacement) assay for K_d determination is significantly more resource demanding and time consuming owing to its low throughput. On the basis of this result, we modified our screening cascade so that the primary hits from both fragment screening (NMR spectroscopy) and HTS were fed directly into the HTS assay for dose–response analysis, instead of using NMR spectroscopy for K_d determination (Figure 3b).

With the progression of such combined fragment screening and HTS, the observed high hit rate and the represented diverse scaffolds led us to decide not to screen the whole compound collection by HTS. In total, we screened approximately 100000 compounds with the HTS assay[34] with a hit rate of approximately 30%. The primary hits from both the fragment screening and the HTS were then evaluated jointly by dose–response analysis (Figure 3b) and subsequent structure-based classification for chemical expansion (see below).

It is remarkable to note that such a high proportion of the fragment hits (identified as binders) showed clear inhibition in the biochemical assay (RapidFire-MS), as reflected by the excellent correlation between the two assays (Figure S4). Our result is consistent with the observation that NMR spectroscopy is the most robust technique for fragment screening.[35] This is an important example showing that rigorous early cross validation between biochemical and biophysical assays can guide the implementation of a more efficient screening cascade for hit finding in lead generation.

Structure-based hit classification for integrated lead generation

For confirmed actives, compounds were selected for crystallization trials. The selection was made initially to map the binding pocket, but it was subsequently shifted to a structure-based classification of the hit series. The selection was done from an affinity ranked hit list by taking into account the chemical tractability and supposed novelty. Clustering methods based on molecular graphs were not employed, as fragment-sized molecules, in contrast to HTS-sized compounds, less frequently share an actual 3D binding mode within such a 2D cluster. The clustering was simply done by a 3D overlay of the experimental crystal structures of sEH in complex with selected fragments. From the initial set of crystal structures, analogues were selected for testing in an iterative approach.

Compared to a traditional HTS, this process placed much higher weight on the use of the structure information to guide the hit evaluation. Interesting hits judged solely on their chemical structures were not pursued further unless the X-ray structure of its ligand complex could be obtained. Such structure-based hit series were then prioritized for further expansion by

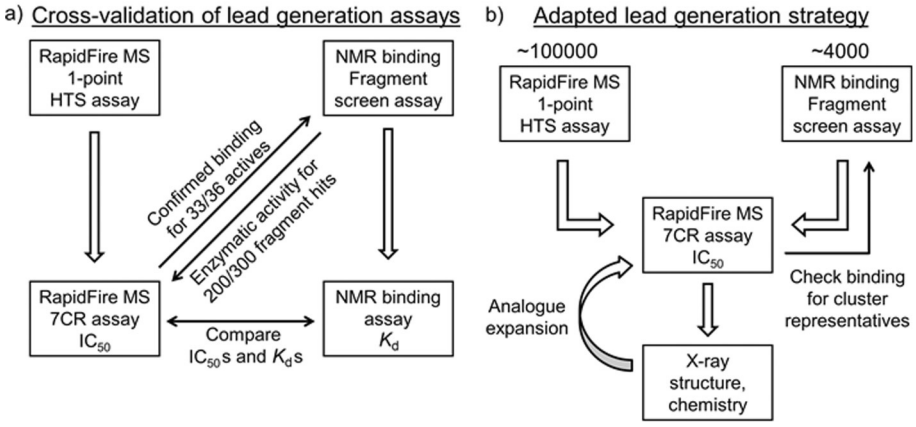

Figure 3. Schematic diagram for a) the cross validation of assays and b) the adapted screening cascade used for hit finding and hit expansion. 7CR assay refers to 7-concentration dose–response analysis.

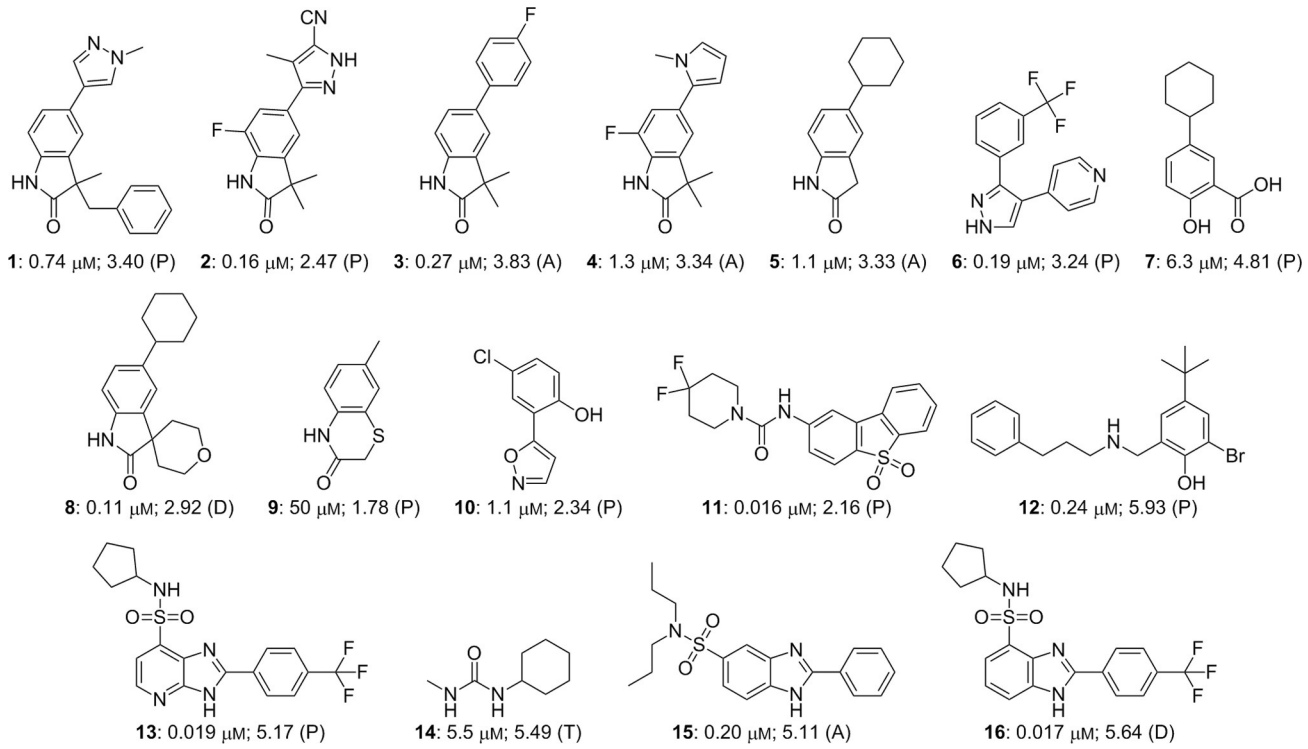

Figure 4. List of compounds from the prioritized series including some tool compounds. The IC_{50} [μM] and cLog*P* values are indicated. The hits are also labeled as primary hit (P), analogue (A), tool compound (T), or designed compound (D). Series are classified primarily based on their 3D binding modes as determined by X-ray crystallography (refer to main text for details). Series 1 is represented by compound **2** (with active analogues **3**–**5** and synthesized **8**), series 2 is represented by compounds **9** and **10**, and series 3 is represented by compounds **11**–**13** (active analogues **15** and synthesized **16**). Compounds **1**, **6**, and **7** were used for comparison for series 1.

consideration of their chemical tractability and structure novelty (see Figure 4 and the discussion below).

Overall shape of the active-site pocket and key interactions of soluble epoxide hydrolase inhibitors

The active-site pocket of sEH displays a dumbbell shape, with three active-site residues, Asp335, Tyr383, and Tyr466, located in the central channel "holding" the midpoint of the handle.[23,31] On the basis of the ligand–complex structures available from the PDB, all existing sEH inhibitors bind by penetrating the central channel with their urea-like motifs engaged in H-bonding interactions with the active-site residues (Figure 5). However, the flanking groups on either side of the inhibitors rarely engage in significant polar interactions, and they spread widely to cover the whole volume in the pocket. For the sake of convenience, we will use the picture in Figure 5 as the standard viewing orientation. In this view, the Phe267 pocket as referred to in the literature[23] is part of the right-hand side (RHS) pocket. Likewise, the Trp336 pocket that is adjacent to the left of the central channel would be part of the left-hand side pocket (LHS).

Identifying important key hot spots of fragment binding

Our crystallographic effort started with the aim to completely map the active-site pocket with experimental structural data to

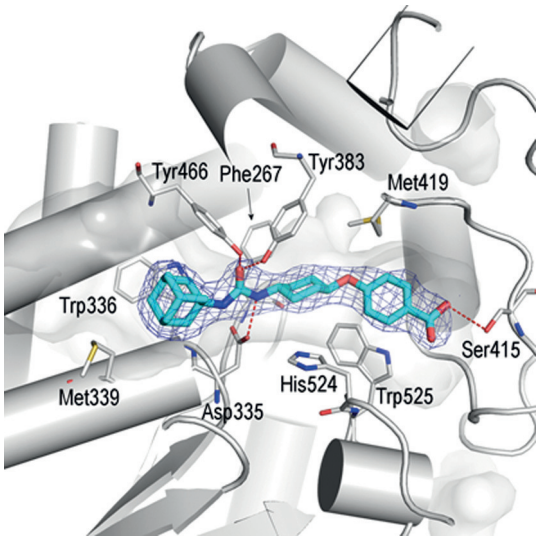

Figure 5. Electron density and binding mode for 4-[4-(1-adamantylcarbamoylamino)cyclohexoxy]benzoic acid[15] (PDB ID: 5AM3[32]). Note that 5am3 will be used to refer to the bound ligand here and the same scheme will be used for all cited PDB structures throughout the paper (i.e., small letters of the PDB ID to refer to the respective bound ligand). The density is shown as the calculated $2F_o-F_c$ map contoured at 1 σ. Note that the urea motif is H-bonded to the active-site residues Asp335, Tyr383, and Tyr466. The end carboxylate is H-bonded to Ser415. This view of the active-site pocket will be used as the default orientation throughout the paper. The Trp336 and Met339 residues are indicated in the LHS, whereas Phe267, Met419, Ser415, His524, and Trp525 are located in the RHS.

gain deeper knowledge of the ligand interactions to guide rational structure-based design discussions. Therefore, a large number of literature compounds and diverse series of confirmed fragment hits were fed into our crystallographic process. In total, more than 50 structures of ligand complexes of sEH were obtained, which provided a comprehensive experimental mapping of the active-site pocket in terms of protein–ligand interactions.[26] Superposition of the bound ligands in these structures resulted in the same dumbbell shape as that in the active-site pocket (Figure 6).

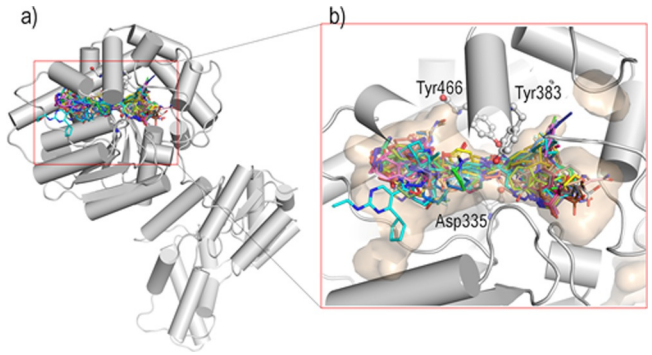

Figure 6. Overall shape of the active-site pocket with an overlay of sEH inhibitors or binders. The active-site residues are depicted as ball-and-stick models. a) Cartoon models of sEH showing the overall fold and the active-site pocket in red box; b) close-up view of the active-site pocket with bound ligands overlaid from 52 structures.[32]

Through this analysis, it became clear that there are certain preferred binding regions with some consensus hot spots, in addition to the central channel (Figure 7a). In comparison, the LHS seems to be mostly occupied by larger hydrophobic groups (Figure 7b).

On the other hand, fragments bound to the RHS mostly align well in space with their aromatic ring structures in a stacking position to the imidazole ring of the His524 residue (Figure 5). Such π stacking to His524 has been observed previously, although no polar interactions were associated with the stacking.[21] Furthermore, two polar interactions to the protein seem to be important (Figure 7c). The majority of bound fragments on this side seem to have both or at least one of these interactions.

Identifying induced-fit binding

For the fragment hits that bind to the central channel, all showed interactions to the active-site residues (Figure 7a). We also determined the ligand–complex structure with compound **13** at 2.57 Å resolution (Figure S11 f). If the binding scaffold is a ring structure (e.g., see compound **13**), certain movements of the protein residues need to take place to accommodate the ligand. Significantly larger induced fit was found for compound **13** (Figures 4 and 8). In this case, the side chain of Tyr383 (OH) has to move approximately 2 Å to allow the imidazole ring of the ligand to enter the central channel. There are no clear polar interactions to the sulfonamide group, and the

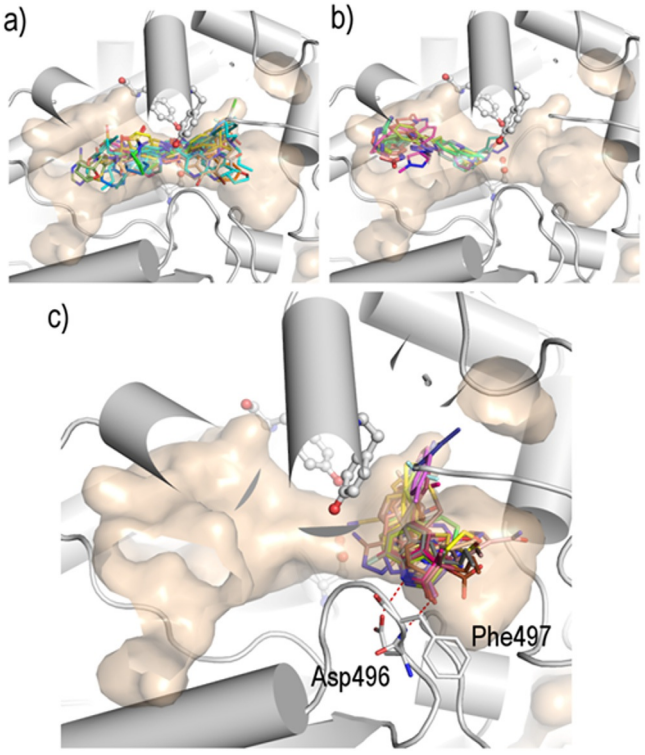

Figure 7. Superposition of ligands that bind to different regions of the pocket: The active-site residues are depicted as ball-and-stick models to indicate the central active-site channel. a) Compounds that bind through the central channel; b) fragment hits that bind at the LHS; c) fragment hits that bind at the RHS. There are two conserved H-bonds to the protein, as indicated by the dashed lines (one to the side chain of Asp496 and the other to the backbone NH of Phe497).

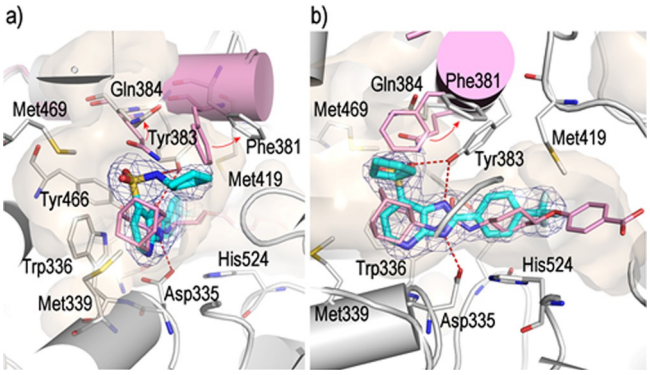

Figure 8. The unique binding mode and electron density for compound **13** (in cyan), 5am3 (in pink) is overlaid for comparison. The electron density is shown as blue mesh for bound **13** ($2F_o-F_c$ map contoured at 1 σ). The nearby Phe381 and Gln384 residues have to move (e.g., up to 5 Å for the phenyl group of Phe381, which would otherwise collide with the cyclopentyl group) to accommodate the bulky structure caused by the 7-sulfonamide kink. In fact, significant portions of the secondary structure including part of the upstream helix (in pink) and a loop region (residues 375–379) became disordered in the crystal. The hydroxyl group of Tyr383 is H-bonded to the sulfonamide nitrogen. The imidazole[4,5b]pyridine ring is in a stacking position to the side chain of Trp336 and is also close to Met339. a) Side view; b) front view (90° apart from a).

cyclopentyl group seems to open a new hydrophobic pocket near Phe381 (Figure 8). Similar induced-fit features were also observed for compound **16**, for which the complex structure was solved at 2.35 Å resolution. Interestingly, the binding mode of compound **15** (which has 2-phenylbenzimidazole-5-sulfonamide as the core, Figure S10b) did not show any induced-fit features. It is evident that such induced-fit binding depends on the specific substitution pattern of the benzimidazole ring. This feature of significant induced fit near the central channel has not been reported previously,[26] and it can be a new direction for sEH inhibitor design. Another region that showed induced-fit binding of ligands is the 410s loop (see below). Notably, compound **13** was identified from the HTS, although hits with the same scaffold were also found in the NMR spectroscopy screening (from the targeted library, see below). The observation regarding protein flexibility upon binding of fragments is in line with a recently reported example on mitochondrial branched-chain aminotransferase,[36] for which it was shown that combined fragment screening and HTS enabled identification of the hit series with novel induced-fit interactions.

Oxoindoline was identified as a novel hit series with polar interactions to the right-hand side

On the basis of their binding modes and overlay with literature sEH inhibitors, we selected three major series (i.e., prioritized series) for further hit expansion and lead generation (Figure 4). From the primary hits, series 1 is represented by compound **2** (with active analogues **3**–**5** and synthesized **8** from the hit expansion), series 2 is represented by compounds **9** and **10**, and series 3 is represented by compounds **11**–**13** (active analogue **15** and synthesized **16**). Compounds **1**, **6**, and **7** were used for comparison for series 1. Below, we briefly describe the chemistry exploration of the respective series.

For series 1, it is most striking to see that compounds **1** and **2**, given their same core scaffolds, bind in completely different regions (≈15 Å apart) in the pocket: **1** binds at the LHS (Figure S11a), whereas **2** binds at the RHS by π stacking to His524 and is H-bonded to Asp496 and Phe497, which are part of the identified hot spots (Figure 7c; see also Figure S11b). For compound **1**, the 3-benzyl group seems to be too big to fit into the RHS pocket (hence preventing its binding to the RHS), and this indicates that the 3D binding mode of the ligand is sensitive to the specific substitution scheme, even with the same core scaffold. For compound **2**, its pyrazole moiety seems mainly to fill up the Phe267 pocket[21] and to interact with the central channel indirectly through a bridging water molecule to Asp335. The Phe267 pocket is occupied by other known sEH inhibitors[5,21,25,26,37] (Figure 9a; see also Figure S1). We reasoned that the significant polar interactions observed for **2** can be used for further chemistry efforts to test the idea that new leads can be generated without interactions to the central channel.

We then searched our in-house compound collection to identify structural analogues to **2** and similar structural motifs and tested them in our RapidFire-MS assay. A total of 107 compounds were selected and 84 were tested. More than 80% were found to be active. Among the active analogues, complex structures with **3**, **4**, and **5** were determined (Figure 9b). As seen for other more potent inhibitors (e.g., 3i1y, Figure S1), the groups occupying the Phe267 pocket seem to prefer an out-of-plane/perpendicular orientation relative to the oxoindoline system.

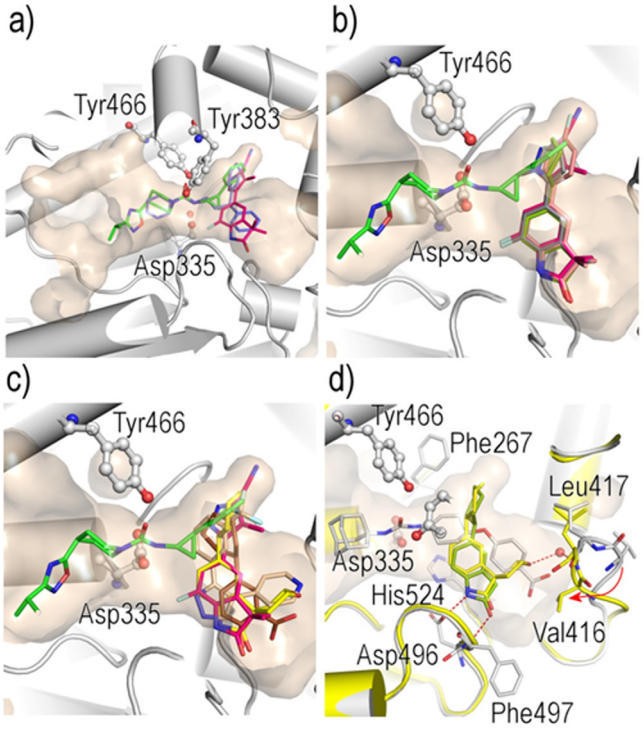

Figure 9. Overlay and comparison of series 1 and literature compounds.[21,25] a) Overlay of **2** (pink) with 3ant (green) and 3i1y (blue); b) overlay of **2** (purple), **3** (pink), **4** (grey), **5** (light green), and 3ant (green); c) overlay of **2** (pink), **6** (beige), **7** (brown), **8** (yellow), and 3ant (green); d) overlay of **8** (yellow) and **6** (light green) showing the polar interaction between **8** and the 410s loop, which moves towards the bound ligand. 5am3 is shown as gray models. The 410s loop collapses upon binding of **8**, which induces large movement around Val416 (≈4 Å for the Cα as indicated by the red arrow). 3ant, 3i1y are literature inhibitors, see Figure S1.

For our design hypothesis, we also compared series 1 with other fragment hits. Compound **6** displays potency similar to that of **2**, although **6** has only one H-bond to the protein (Figure 9c). Notably, the nitrogen atom of the pyridine ring interacts with the 410s loop through a bridging water molecule. Compound **7** has a phenol moiety as the core scaffold and is H-bonded, through its hydroxyl group, to the protein (Phe497) (Figure 9c). Most interesting is the observation that the carboxylate group from **7** occupies a part of the RHS pocket that is similar to that occupied by the pyridine ring in **6**. We consider this region as a potential direction from which we can further explore by adding relevant bulky substituents to form polar interactions. Compound **8** was synthesized to test such a design hypothesis, and its complex structure with sEH was also determined (Figure 9d). The cyclohexyl group is virtually superimposed on top of that of **5** but with a 180° flip; this can likely be attributed to the large size of the tetrahydropyran

ring, which is in a chair configuration with the ring oxygen atom interacting with Ser407 and Leu417 through a bridging water molecule (Figure 9d; see also Figure S10c). Interestingly, the 410s loop seems to have "collapsed" towards **8** with Val416 flipped from an outward position to an inward position. This illustrates that the RHS pocket possesses a certain level of flexibility (i.e., is able to constitute induced-fit binding to some ligands).[32] The binding mode of **8** to a large extent confirmed our design hypothesis, which provided good basis for further chemistry exploration.

For series 2, we included **9** and **10** as representatives. Both bind at the RHS pocket with π stacking to His524 but with different core scaffolds (Figure 10a). They are coplanar to each other in the superposition and approximately overlap the end groups of the literature inhibitors 1zd2, 1zd5, 3koo, and 4jnc

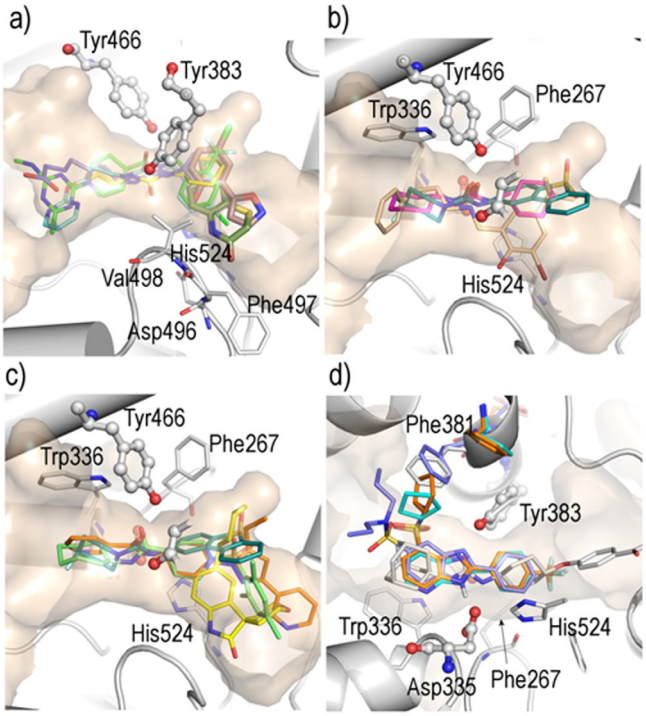

Figure 10. a) Overlay of series 2 with literature compounds: **9** (deep green), **10** (brown), 1zd2 (yellow), 1zd5 (blue), 3koo (cyan), and 4jnc (green)[23,38,39]. Binding modes for series 3: b) overlay of **12** (beige), **11** (blue), and **14** (purple); c) overlay of **11** (blue), **8** (yellow), 3otq (orange), and 4hai (light green);[40,41] d) overlay of **15** (blue), **13** (cyan), **16** (orange), and 5am3 (white). 1zd2, 1zd5, 3koo, 4jnc, 3otq, and 4hai are literature inhibitors, see Figure S1.

(Figure 10a; see also Figure S1). Interestingly, the isoxazole part of **10** seems to mainly fill up the space of the RHS pocket with its ring nitrogen atom in contact with the solvent molecules. Relative to the potency of **5** (series 1), that of **9** is significantly lower (≈50-fold based on the IC_{50} value); this decrease in potency is likely due to weakened H-bonds to the Asp496 residue (distance changes from 2.7 to 3.2 Å) and the Phe497 residue (from 2.8 to 3.1 Å) in addition to the much smaller group at the Phe267 pocket. In summary, we found that the main binding mode for series 2 involves a planar structure without strong polar interactions. Given that this did not offer any clear route for chemistry expansion, we decided not to pursue this series further.

2-Phenylbenzimidazole-4-sulfonamide was identified as a hit series with novel interactions to the central channel

For series 3, we wanted to explore the hits that penetrate the central channel but that have distinct features. Compound **12** is interesting, as it interacts with the central channel and is also H-bonded to Asp496 through its phenolic hydroxyl group (Figure 10b). Unlike previous sEH inhibitors, **12** has a secondary amine group instead of a urea-based motif. Furthermore, compared to series 1, the substituted phenyl moiety approximately overlaps the benzene ring of the oxoindoline system, and the *tert*-butyl group superposes the 5-substituent of the oxoindoline ring well (Figure 10b,c). We speculate that it might be possible to combine these two features to a new lead series that makes significant polar interactions in the RHS pocket and to the central channel (Figure 10c). Compound **11** has a urea-based motif, that is, a piperidine-1-carboxamide moiety, as previously reported[25,38] (e.g., 3ant and 3koo, see Figure S1). However, the large substituent in **11**, that is, the dibenzothiophenesulfone moiety, occupies the Phe267 pocket mainly with a hydrophobic and space-filling function.

Inhibitors with larger hydrophobic groups occupying the RHS pocket include an amide-based pyrazole[40] and a piperidine derivative[41] (3otq and 4hai, see Figure S1), which are both oriented perpendicular to the dibenzothiophenesulfone moiety in **11** (Figure 10c). It would be desirable to combine this large hydrophobic functionality with the features of series 1. Next, we turned to the most interesting hit from series 3. Compound **13** has an imidazo[4,5-*b*]pyridine group that binds to the central channel with significant induced fit (Figure 10d). Its potency is nearly 10-fold better (IC_{50} = 19 nM) than that of **2** from series 1 (IC_{50} = 160 nM). Compound **15** was tested as an active analogue; it has a benzimidazole core scaffold. Changing from a 4-substituent to a 5-substituent eliminated the need for a large rearrangement around the LHS pocket (Figure 10d). Furthermore, owing to its smaller end group (unsubstituted phenyl group at the 2-position of the benzimidazole ring), compound **15** shows much weaker binding (10-fold difference in IC_{50} value; Figure 4) than **13** and displays dual binding modes similar to **14** (Figure S10), which indicates that the aliphatic tail on the 5-sulfonamide unit can fit in either side of the pocket with no clear discrimination. We envisage that structures represented by **13** can be used as a starting point for new sEH inhibitors. As an initial attempt, **16** was designed to simplify the ring structure and to test a more feasible synthesis. Compounds **16** and **13** only differ by one atom (benzene versus pyridine ring) and show similar potency (IC_{50} = 17 and 19 nM). To validate our design, we also obtained the complex structure for **16**. The only difference relative to **13** is the orientation of the cyclopentyl group, which is rotated in **16** by approximately 80° around the sulfonamide S–N bond (Figure 10d), likely as a result of differences in the electronic properties.

It was reported in 2012[42] that in animal models the inhibitors of sEH elevated endogenous EET levels and promoted primary tumor growth and metastasis. Owing to the potential liability of such a target-related tumorigenesis effect, the sEH project at AstraZeneca was terminated and our lead generation effort was stopped prematurely. No further work was conducted.

After the closing phase of this project, 2-phenylbenzimidazole and related derivatives were reported as fragment hits for sEH on the basis of elaborate in silico approaches.[27,43] Whereas the best 2-phenylbenzimidazole compound from those in silico screenings has a potency in the low micromolar range, compound **16** as a representative of our 2-phenylbenzimidazole-4-sulfonamides has significantly higher potency (IC_{50} = 17 nM). More importantly, the induced-fit features associated with the 2-phenylbenzimidazole-4-sulfonamide scaffold as revealed by high-resolution crystal structures present distinct novel interactions with sEH.

Retrospective analysis of hits from the fragment screening and the high-throughput screening

Given that both the fragment screening and the HTS gave high hit rates, we wanted to understand how these two screening campaigns contributed to the hit series identified. Therefore, we performed a retrospective analysis of the prioritized series by looking at their origins, NMR spectroscopy screening versus HTS as the primary screening, as well as targeted versus generic libraries in the case of NMR spectroscopy screening.

For the NMR spectroscopy screen, the 2-phenylbenzimidazole scaffold in series 3 was enriched significantly by the targeted selection (Figure 4 and Table 1). This series showed novel interactions to the central channel and afforded a potential new scaffold for sEH inhibitors. However, this scaffold was not found among the hits from the generic fragment library, whereas three such hits were identified from the targeted library. One clear difference between the generic and the targeted libraries lies in their mean molecular weights (MWs, 159 vs. 210 Da); this may be a reasonable explanation for the above observation. Indeed, it was found that compounds bearing the 2-phenylbenzimidazole group (MW: 194 Da for the core scaffold) simply did not exist in the generic library.

Looking at the hits from NMR spectroscopy and HTS, the scaffolds in series 1 and 3 showed comparable hit rates for both screens (roughly proportional to the number of compounds tested in the respective screens (i.e., total ≈4000 vs. ≈100 000, which gives 4:100, Table 1). However, there is a trend that series 2 seems to be significantly over-represented from the fragment screening (e.g., hit ratio 60:100 between the fragment screening and HTS for the benzothiazinones) than other scaffolds. This could be due to the fact that the core scaffolds of series 2 (MW: ≈170 Da) are more enriched in the fragment libraries than the HTS collection. In contrast, series 3 (the 2-phenylbenzimidazole-4-sulfonamide scaffold) was also found among the HTS hits but not from the generic fragment library. This is consistent with the fact that the HTS compounds have a size distribution towards larger MWs. Notably, the most potent 2-phenylbenzimidazole-4-sulfonamide compound from HTS (compound **13** in Figure 4) has a MW of approximately 410 Da.

It should also be pointed out that the NMR spectroscopy hits are much less potent than the hits from the HTS (e.g., the best 2-phenylbenzimidazole hit from NMR spectroscopy has an IC_{50} value of 185 μM, which is ≈10 000-fold less potent than compound **13**). Without the HTS hits, it would probably have limited our chance to obtain the structure information for this scaffold. As we had concluded from earlier analysis, the success rate to obtain complex structures seems to be directly correlated to their affinity in the case of sEH, for example, only 35% success rate if the affinity is weak with an IC_{50} value higher than 100 μM.[32] Given the fact that we were relying on the structure information to guide the hit evaluation, this scaffold might not be prioritized if we had not gotten the complex structure with **13** (which originated from HTS).

Conclusions

Through a combination of fragment screening and high-throughput screening, that is, a parallel primary screening followed by integrated hit-confirmation and structure-based hit evaluation, we identified two scaffolds, oxoindoline and 2-phenylbenzimidazole-4-sulfonamide, as new chemical series for potential soluble epoxide hydrolase inhibitors. With our initial chemistry effort, we demonstrated that the oxoindoline series can be further expanded by retaining the polar interactions to the right-hand side (H-bonds to Asp496 and Phe496), and specific interactions can be introduced to target the 410s loop region by induced fit. In addition, we showed that the 2-phenylbenzimidazole-4-sulfonamide series seem to afford synthetic feasibility for further work. On the basis of the encouraging initial results, we envision that a new lead series with improved

Table 1. Origin of the key scaffolds versus number of hits in the prioritized series.

Series	Scaffold	Representative compound[a]	NMR hits		Total hits	
			generic library	targeted library	NMR	HTS
1	oxoindoline	**2**	4	2	6	>80
2	benzothiazinone	**9**	2	1	3	5
	phenylisoxazole	**10**	1	2	3	20
3	2-phenylbenzimidazole	**13**	0	3	3	>40

[a] See Figure 4 for structures of the primary hits.

properties (especially physicochemical properties) could be generated if we combine features from 5-cyclohexylspiro[indoline-3,4′-tetrahydropyran]-2-one (**8**) and *N*-cyclopentyl-2-[4-(trifluoromethyl)phenyl]-1*H*-benzimidazole-4-sulfonamide (**16**). The main challenge would be to find a vector that can merge the cyclohexyl functionality of **8** with the trifluoromethyl moiety of **16** (red circle in Figure 11). With the rich structure information, we envisage that functional groups such as sulfonamides or large aliphatic ring systems could be tested as potential candidates for such a purpose.

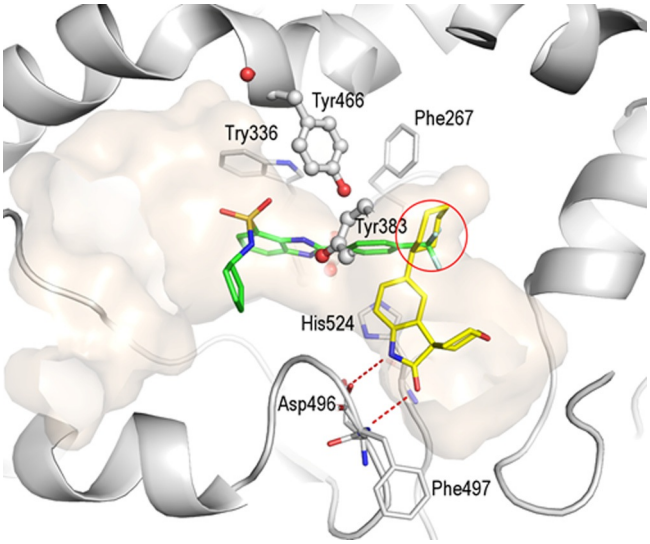

Figure 11. Overlay of compounds **8** (yellow) and **16** (green) binding to sEH. The red circle indicates the overlap of the cyclohexyl group of **8** and with the trifluoromethyl moiety of **16**.

The present work illustrates the importance of early cross validation of the different assays, as this guided us to adapt the screening cascade. The cross validation was then followed by an integrated hit evaluation by using a structure-based approach, as we initially planned. Such an integrated strategy enabled an effective hit-finding process that resulted in a number of hit series with distinct interactions to soluble epoxide hydrolase.

Experimental Section

General comments: 11,12-Epoxy-(5*Z*,8*Z*,14*Z*)-eicosatrieonic acid (11,12-EET) and 11,12-dihydro-(5*Z*,8*Z*,14*Z*)-eicosatrieonic acid (11,12-DHET) were obtained from Caman Chemicals. Human soluble epoxide hydrolase (sEH) was prepared in house. All other chemicals were from Sigma, unless otherwise stated. Complete details of the protein constructs and recombinant production are given in the Supporting Information.

Library selection and molecular modeling

Generic screening library: The AstraZeneca (AZ) general fragment library currently comprises about 16000 compounds. Out of these, compounds with no more than 12 heavy atoms (HA) were selected, which resulted in a set of approximately 3000 compounds. This set was sorted by the heteroatom fraction, which was followed by a thorough visual inspection. The selection of compounds for a generic NMR spectroscopy screening library resulted in a set of 1202 compounds with a mean MW of 159 Da. Some basic statistics are given in the Supporting Information. A total of 1195 of these compounds were included in the primary fragment screen by NMR spectroscopy.

Targeted screening library: The targeted fragment screening library was built in the following way. Out of the AZ corporate compound collection, all compounds with no more than 4 rotatable bonds (SciTegic def.), no more than 18 HA, calculated log $D_{7.4}$ (SciTegic def.) lower than or equal to 4, at least 1 ring system, and at least 1 heteroatom were selected, which resulted in approximately 134000 compounds for the targeted virtual screening set I. A second set, the targeted virtual screening set II, comprised all 16000 compounds in the AZ general fragment library. Both sets were converted separately into conformational ensembles of 3D structures for virtual screening. First, for all unique compounds protonation states were set and tautomers were enumerated as appropriate.[44] All undefined stereochemistry, except on pyramidal nitrogen atoms, was then enumerated, while keeping all defined stereochemical features.[45] Initial 3D models, as well as conformational ensembles were generated by using Omega 2.4.3[46] with these parameters: buidff = mmff94s_NoEstat, enumNitrogen = true, enumRing = true, ewindow = 10.0, maxconfs = 500, rms = 0.5, searchff = mmff94s NoEstat, and an in-house developed torsion angle library.[47] The virtual screening of these compounds was performed as a rigid docking by using FRED 2.2.5.[48] Each of the two targeted virtual screening libraries was docked separately by using a total of 20 boxes, derived from 7 fragmentations differing in size and covered space of a reference compound [PDB ID: 3I28, re-refined].

For each run separately, all hits were ranked by consensus scoring with Chemgauss3, OEChemscore, and PLP, this way discarding the worst poses by agreement of multiple different scoring functions, rather than simply selecting the "top *n*" solutions for any single-scoring function. The targeted screening sets I and II resulted in 4636 and 3630 compound hits, respectively. Of these, 55 and 85% were, respectively, kept by random selection, which resulted in a pooled set of 5821 virtual screening hits on a unique compound level.

The targeted screening library was then finalized by several rounds of thorough visual inspection and selection, which resulted in a targeted NMR screening library of approximately 3000 compounds. The initial set of 5821 compounds showed a mean MW of 210 Da. Some basic statistics are given in the Supporting Information. After several rounds of careful visual inspection, a subset of 2861 compounds was included in the primary fragment screen by NMR spectroscopy. For further details of the method and a discussion, refer to the Supporting Information.

Molecular modeling: Proteins were prepared by using Schrödinger software,[49] 3D models were generated by using CORINA,[45] and flexible dockings were performed with GOLD[50] by writing out all poses for subsequent post-processing. For full details, refer to the Supporting Information.

Fragment screening by NMR spectroscopy

The NMR spectroscopy experiments were conducted with a Bruker 600 or 800 MHz spectrometer equipped with a cryogenically

cooled TXI-probe head. A SampleRail™ sample delivery system (Bruker BioSpin) connected the spectrometer with a Tecan sample preparation robot. Each protein or ligand addition was done just prior to the NMR spectroscopy experiment. To avoid dilution with robot system liquid (water), an in-house constructed piston was used for mixing the sample in the NMR tube. Ligand binding was detected by using 1D ^{1}H CPMG NMR spectroscopy experiments acquired at 293 K with 256 scans and a repetition delay of 3 s. The CPMG spin echo part of the sequence consisted of 96 pulses with 180° flip angle, interspaced by 2 ms, to give a spin lock time of 196 ms. A dual selective pulse (shape sinc1, 3 ms) was used in the excitation-sculpting scheme to suppress both the residual water and DMSO signals simultaneously.[51] The NMR spectroscopy data was processed with 2 Hz line broadening and base-line correction. The resonance integrals were extracted by using TopSpin (Bruker). The dissociation constants obtained from the mutual titration experiments were determined by using the Levenberg–Marquardt least-squares optimization[52] in Matlab (Mathworks Inc., implemented by Kristofer Modig, unpublished results). The uncertainties in the fitted parameters ($K_{d,1}$, $I_{min,1}$, $I_{max,1}$, $K_{d,2}$, $I_{min,2}$, and $I_{max,2}$) were estimated by scaling the experimental error to give a reduced $\chi^2 = 1$.

Fragments were screened from cocktails containing six compounds (prepared in a randomized way) each at a concentration of 50 μM. The concentration of reference compound [1-(1-adamantyl)-3-(1-methylsulfonyl-4-piperidyl)urea,[15] Figure 2] was 50 μM. Analysis of the fragment screening was done by overlaying the spectra of the fragment mixture, the fragment mixture in the presence of the protein, and the fragment mixture in the presence of the protein and the strong inhibitor in TopSpin (Bruker). Fragment hits were identified by comparison with prerecorded reference spectra of all fragments. Fragments showing at least 40% decrease in signal intensity and a substantial regain of signal intensity upon addition of the reference compound were regarded as hits. The buffer was 50 mM deuterated Tris pH 7.5, 50 mM NaCl, 10% D_2O. The protein stock concentration was 100 μM.

NMR spectroscopy determination of the K_d values of the fragments was performed by using a 1D NMR reporter displacement assay. The reporter signal intensity recovery was monitored using a CPMG experiment. The K_d values were calculated from equations derived for a three-component competitive equilibrium model involving the reporter, the test compound, and protein relating the signal recovery to the concentration of the competing fragment. For more details, refer to the Supporting Information.

HTS screening

Plate set up: For the HTS screen, the compound (40 nL) was added to a 384 Greiner polystyrene plate by using an acoustic dispenser (Ecco, Labcyte). The enzyme (20 μL) in 50 mM Tris, pH 7.4, was added to the plate (Mulitdrop); the mixture was pre-incubated for 15 min and then 11,12-EET (20 μL) (Multidrop) was added, and the reaction was allowed to incubate for 30 min. The reaction was stopped by adding water (40 μL) containing a strong inhibitor (Multidrop). Final concentration was 5 nM enzyme, 1 μM 11,12-EET, and 20 μM inhibitor.

RapidFire-MS: The plates was loaded into a RapidFire 300 (Agilent Technologies) coupled to an API 4000 mass spectrometer (SCIEX). Buffer A: 0.2% formic acid in water and buffer B: 0.2% formic acid in methanol. Samples were loaded onto a C18 column and nonvolatile components was removed by washing the column with buffer A. Elution of 11,12 EET and 11,12-DHET was done by using buffer. Detection was performed by using the positive ESI MRM mode with the following transitions: 11,12-EET 321.3/303.2 and 11,12-DHET 339.2/135.

The ratio (R) of substrate (S) to product (P) was calculated by using Equation (1). The percentage effect of a compound's ability to inhibit the enzyme was calculated by using Equation (2). In the spot test (single concentration at 20 μM), a tested compound that showed at least 30% inhibition was regarded as a hit.

$$R = \frac{P}{(P + S)} \quad (1)$$

$$\% \text{ Effect} = 100 \times \frac{(I - \text{DMSO})}{(\text{control} - \text{DMSO})} \quad (2)$$

in which DMSO is the ratio for the well containing only DMSO and control is the ratio for the well with a strong inhibitor (I).

Crystallization and structure determination

For detailed experimental procedures, refer to Ref. [32]. The structure with compound **16** was obtained by co-crystallization. Apoprotein (18 mg mL^{-1}) was mixed with the compound to a concentration of 5 mM and was incubated at room temperature for 3 h. Thereafter, crystals were setup in the same manner as for the apoprotein and were flash frozen without any addition of cryoprotection.

Structures of the ligand complexes with compounds **1**–**15** were deposited in the PDB with IDs: 5ALO, 5ALY, 5ALN, 5AM0, 5ALD, 5AKH, 5AIA, 5AM4, 5AIC, 5ALE, 5AKE, 5AI9, 5ALS, 5AKZ, and 5AKF.[32] Details and statistics of data collection and refinement for sEH in complex with **16** are recorded in Table S1. The atomic coordinates and the structure factors of this sEH complex were deposited in the protein data bank (www.pdb.org) with PDB ID: 5FP0.

PYMOL[53] was used for structure comparison and preparing figures. Note that capital letters are used for the PDB IDs and the same IDs in small letters are used to refer to the ligand bound in that structure.

Synthetic chemistry

Chemicals and solvents from commercially available sources were purchased and used without further purification. ^{1}H NMR spectra were recorded with a Bruker Biospin GmbH 400, 500, or 600 MHz spectrometer. Chemical shifts are reported in parts-per-million (δ) relative to [D_6]DMSO at $\delta = 2.50$ ppm, $CDCl_3$ at $\delta = 7.26$ ppm, or CD_3OD at $\delta = 3.31$ ppm as an internal standard. All tested compounds were purified to >95% purity, as determined by ^{1}H NMR spectroscopy and HRMS or HPLC–UV. Heating of reactions with microwaves was performed with a Biotage Initiator 2.45 GHz, 400 W microwave for the times indicated. Compounds in Figure 4 (except **3**, **4**, **8**, and **16**) were obtained from the AstraZeneca corporate compound collection. Experimental and spectroscopic details for noncommercially available compounds **3**, **4**, **8**, and **16** are described in the Supporting Information. In general, optimizations of the reaction procedures were not performed and yields are given for isolated materials.

Author contributions

S.B. performed the experiments on protein production; H.-G.B. performed the computational studies for fragment library design and hit evaluation; C.A.J. performed the NMR spectroscopy experiments; L.Ö. performed the crystallization experiments; M.R. performed the HTS and dose–response analyses; D.K. participated in the medicinal chemistry design and hit evaluation; T.O. led medicinal chemistry and the hit evaluation and wrote the Introduction; Y.X. performed the structural analyses and comparison and wrote and edited the manuscript; H.-G.B., T.O, and Y.X. participated in the structure-based design; S.B., H.-G.B., C.A.J., L.Ö., M.R., and T.O. wrote the relevant experimental parts; and H.-G.B., C.A. J., L.Ö., and T.O. provided critical reviews.

Acknowledgements

The authors thank Margareta Herslöf for her efforts in the early stages of the project; Erik Olandersson, Kjell Johansson, and Johan Cassel for their work in synthetic chemistry; Anna Öhrn for her contribution in the NMR spectroscopy screening; Gisela Brändén and Gerhard Fischer for their contributions in the early structure work; and Victoria B. K. Ullah for her assistance in retrieving some of the experimental information.

Keywords: drug discovery · high-throughput screening · inhibitors · ligand complex structures · soluble epoxide hydrolase

[1] M. A. Hye Khan, T. S. Pavlov, S. V. Christain, J. Neckar, A. Staruschenko, K. M. Gauthier, J. H. Capdevila, J. R. Falck, W. B. Campbell, J. D. Imig, *Clin. Sci.* **2014**, *127*, 463 – 474.
[2] W. B. Campbell, *Trends Pharmacol. Sci.* **2000**, *21*, 125 – 127.
[3] S. D. Kodani, B. D. Hammock, *Drug Metab. Dispos.* **2015**, *43*, 788 – 802.
[4] K. Sodhi, K. Inoue, K. H. Gotlinger, M. Canestraro, L. Vanella, D. H. Kim, V. L. Manthati, S. R. Koduru, J. R. Falck, M. L. Schwartzman, N. G. Abraham, *J. Pharmacol. Exp. Ther.* **2009**, *331*, 906 – 916.
[5] C. Morisseau, B. D. Hammock, *Annu. Rev. Pharmacol. Toxicol.* **2013**, *53*, 37 – 58.
[6] H. C. Shen, B. D. Hammock, *J. Med. Chem.* **2012**, *55*, 1789 – 1808.
[7] W. K. Lin, J. R. Falck, P. Y. Wong, *Biochem. Biophys. Res. Commun.* **1990**, *167*, 977 – 981.
[8] J. D. Imig, X. Zhao, C. Z. Zaharis, J. J. Olearczyk, D. M. Pollock, J. W. Newman, I. Kim, T. Watanabe, B. D. Hammock, *Hypertension* **2005**, *46*, 975 – 981.
[9] K. G. Maier, R. J. Roman, *Curr. Opin. Nephrol. Hypertens.* **2001**, *10*, 81 – 87.
[10] J. D. Imig, B. D. Hammock, *Nat. Rev. Drug Discovery* **2009**, *8*, 794 – 805.
[11] R. J. Roman, *Physiol. Rev.* **2002**, *82*, 131 – 185.
[12] W. B. Campbell, D. Gebremedhin, P. F. Pratt, D. R. Harder, *Circ. Res.* **1996**, *78*, 415 – 423.
[13] K. G. Proctor, J. R. Falck, J. Capdevila, *Circ. Res.* **1987**, *60*, 50 – 59.
[14] D. Gebremedhin, Y. H. Ma, J. R. Falck, R. J. Roman, M. VanRollins, D. R. Harder, *Am. J. Physiol.* **1992**, *263*, H519 – H525.
[15] Y. X. Wang, L. N. Zhang, G. M. Rubanyi, (Arete Therapeutics, Inc., San Francisco, USA), PCT Int. Pat. Appl. PCT/US2009/053863 (WO 2010025043 A1), **2010**.
[16] "*Evaluation of Soluble Epoxide Hydrolase (s-EH) Inhibitor in Patients with Mild to Moderate Hypertension and Impaired Glucose Tolerance*", clinical trial #NCT00847899 (Sponsor: Arete Therapeutics, Inc.); https://clinicaltrials.gov/ct2/show/NCT00847899.
[17] C. Morisseau, M. H. Goodrow, D. Dowdy, J. Zheng, J. F. Greene, J. R. Sanborn, B. D. Hammock, *Proc. Natl. Acad. Sci. USA* **1999**, *96*, 8849 – 8854.
[18] I. H. Kim, F. R. Heirtzler, C. Morisseau, K. Nishi, H. J. Tsai, B. D. Hammock, *J. Med. Chem.* **2005**, *48*, 3621 – 3629.
[19] S. Anandan, H. K. Webb, D. Chen, Y. Wang, B. R. Aavula, S. Cases, Y. Cheng, Z. N. Do, U. Mehra, V. Tran, J. Vincelette, J. Waszczuk, K. White, K. R. Wong, L. Zhang, P. D. Jones, B. D. Hammock, D. V. Patel, R. Whitcomb, D. E. MacIntyre, J. Sabry, R. Gless, *Bioorg. Med. Chem. Lett.* **2011**, *21*, 983 – 988.
[20] H. C. Shen, F. Ding, S. Wang, S. Xu, H. Chen, X. Tong, V. Tong, K. Mitra, S. Kumar, X. Zhang, Y. Chen, G. Zhou, L. Pai, M. Alonso-Galicia, X. Chen, B. Zhang, J. R. Tata, J. P. Berger, S. L. Colletti, *Bioorg. Med. Chem. Lett.* **2009**, *19*, 3398 – 3404.
[21] A. B. Eldrup, F. Soleymanzadeh, S. J. Taylor, I. Muegge, N. A. Farrow, D. Joseph, K. McKellop, C. C. Man, A. Kukulka, S. De Lombaert, *J. Med. Chem.* **2009**, *52*, 5880 – 5895.
[22] R. H. Ingraham, R. D. Gless, H. Y. Lo, *Curr. Med. Chem.* **2011**, *18*, 587 – 603.
[23] G. A. Gomez, C. Morisseau, B. D. Hammock, D. W. Christianson, *Protein Sci.* **2006**, *15*, 58 – 64.
[24] M. Baker, *Nat. Rev. Drug Discovery* **2013**, *12*, 5 – 7.
[25] D. Tanaka, Y. Tsuda, T. Shiyama, T. Nishimura, N. Chiyo, Y. Tominaga, N. Sawada, T. Mimoto, N. Kusunose, *J. Med. Chem.* **2011**, *54*, 851 – 857.
[26] L. Xing, J. J. McDonald, S. A. Kolodziej, R. G. Kurumbail, J. M. Williams, C. J. Warren, J. M. O'Neal, J. E. Skepner, S. L. Roberds, *J. Med. Chem.* **2011**, *54*, 1211 – 1222.
[27] J. Achenbach, F. Klingler, R. Blöcher, D. Moser, A. Häfner, C. B. Rödl, S. Kretschmer, B. Krüger, F. Löhr, H. Stark, B. Hofmann, D. Steinhilber, E. Proschak, *ACS Med. Chem. Lett.* **2013**, *4*, 1169 – 1172.
[28] D. Moser, J. Achenbach, F. Klingler, B. Estella, S. Hahn, E. Proschak, *Bioorg. Med. Chem. Lett.* **2012**, *22*, 6762 – 6765.
[29] Y. Amano, E. Tanabe, T. Yamaguchi, *Bioorg. Med. Chem.* **2015**, *23*, 2310 – 2317.
[30] M. Whittaker, R. J. Law, O. Ichihara, T. Hesterkamp, D. Hallett, *Drug Discovery Today Technol.* **2010**, *7*, e163 – e171.
[31] C. Dalvit, M. Fasolini, M. Flocco, S. Knapp, P. Pevarello, M. Veronesi, *J. Med. Chem.* **2002**, *45*, 2610 – 2614.
[32] L. Öster, S. Tapani, Y. Xue, H. Käck, *Drug Discovery Today* **2015**, *20*, 1104 – 1111.
[33] S. Meiboom, D. Gill, *Rev. Sci. Instrum.* **1958**, *29*, 688 – 691.
[34] J. W. M. Nissink, S. Schmitt, S. Blackburn, S. Peters, *J. Biomol. Screening* **2014**, *19*, 369 – 378.
[35] R. E. Hubbard, J. B. Murray, *Methods Enzymol.* **2011**, *493*, 509 – 531.
[36] S. M. Bertrand, N. Ancellin, B. Beaufils, R. P. Bingham, J. A. Borthwick, A. Boullay, E. Boursier, P. S. Carter, C. Chung, I. Churcher, N. Dodic, M. Fouchet, C. Fournier, P. L. Francis, L. A. Gummer, K. Herry, A. Hobbs, C. I. Hobbs, P. Homes, C. Jamieson, E. Nicodeme, S. D. Pickett, I. H. Reid, G. L. Simpson, L. A. Sloan, S. E. Smith, D. O. Somers, C. Spitzfaden, C. J. Suckling, K. Valko, Y. Washio, R. J. Young, *J. Med. Chem.* **2015**, *58*, 7140 – 7163.
[37] G. A. Gomez, C. Morisseau, B. D. Hammock, D. W. Christianson, *Biochemistry* **2004**, *43*, 4716 – 4723.
[38] A. B. Eldrup, F. Soleymanzadeh, N. A. Farrow, A. Kukulka, S. De Lombaert, *Bioorg. Med. Chem. Lett.* **2010**, *20*, 571 – 575.
[39] R. K. Thalji, J. J. McAtee, S. Belyanskaya, M. Brandt, G. D. Brown, M. H. Costell, Y. Ding, J. W. Dodson, S. H. Eisennagel, R. E. Fries, J. W. Gross, M. R. Harpel, D. A. Holt, D. I. Israel, L. J. Jolivette, D. Krosky, H. Li, Q. Lu, T. Mandichak, T. Roethke, C. G. Schnackenberg, B. Schwartz, L. M. Shewchuk, W. Xie, D. J. Behm, S. A. Douglas, A. L. Shaw, J. P. Marino, Jr., *Bioorg. Med. Chem. Lett.* **2013**, *23*, 3584 – 3588.
[40] H. Y. Lo, C. C. Man, R. W. Fleck, N. A. Farrow, R. H. Ingraham, A. Kukulka, J. R. Proudfoot, R. Betageri, T. Kirrane, U. Patel, R. Sharma, M. A. Hoermann, A. Kabcenell, S. D. Lombaert, *Bioorg. Med. Chem. Lett.* **2010**, *20*, 6379 – 6383.
[41] S. Pecic, S. Pakhomova, M. E. Newcomer, C. Morisseau, B. D. Hammock, Z. Zhu, A. Rinderspacher, S. Deng, *Bioorg. Med. Chem. Lett.* **2013**, *23*, 417 – 421.
[42] D. Panigrahy, M. L. Edin, C. R. Lee, S. Huang, D. R. Bielenberg, C. E. Butterfield, C. M. Barnes, A. Mammoto, T. Mammoto, A. Luria, O. Benny, D. M. Chaponis, A. C. Dudley, E. R. Greene, J. A. Vergilio, G. Pietramaggiori, S. S. Scherer-Pietramaggiori, S. M. Short, M. Seth, F. B. Lih, K. B. Tomer, J. Yang, R. A. Schwendener, B. D. Hammock, J. R. Falck, V. L. Manthati, D. E. Ingber, A. Kaipainen, P. A. D'Amore, M. W. Kieran, D. C. Zeldin, *J. Clin. Invest.* **2012**, *122*, 178 – 191.

[43] D. Moser, J. M. Wisniewska, S. Hahn, J. Achenbach, E. Buscató, F. Klingler, B. Hofmann, D. Steinhilber, E. Proschak, *ACS Med. Chem. Lett.* **2012**, *3*, 155 – 158.
[44] Permute (version 0.8-4), proprietary software, AstraZeneca.
[45] Molecular Networks GmbH, Erlangen, Germany; www.molecular-networks.com.
[46] Omega version 2.4.3, OpenEye Scientific Software, Santa Fe, USA; www.eyesopen.com/omega; P. C. D. Hawkins, A. G. Skillman, G. L. Warren, B. A. Ellingson, M. T. Stahl, *J. Chem. Inf. Model.* **2010**, *50*, 572 – 584.
[47] J. Sadowski, J. Bostrom, *J. Chem. Inf. Model.* **2006**, *46*, 2305 – 2309.
[48] FRED version 2.2.5, OpenEye Scientific Software, Santa Fe, NM (USA); www.eyesopen.com/oedocking.
[49] Schrödinger Release 2014-1: Maestro, Version 9.7, Schrödinger LLC, New York, NY, **2014**.
[50] G. Jones, P. Willett, R. C. Glen, A. R. Leach, R. Taylor, *J. Mol. Biol.* **1997**, *267*, 727 – 748.
[51] T. L. Hwang, A. J. Shaka, *J. Magn. Reson. Ser. A* **1995**, *112*, 275 – 279.
[52] J. Pujol, *Geophysics* **2007**, *72*, W1 – W16.
[53] D. Warren, *The PyMOL Molecular Graphics System*, Version 1.3, Schrödinger LLC.

Received: December 11, 2015
Published online on February 4, 2016